

## Vinen's Energy Barrier

Barenghi, C. F.; McClintock, P. V. E.; Muirhead, C. M.

DOI:

[10.1007/s10909-023-02945-7](https://doi.org/10.1007/s10909-023-02945-7)

License:

Creative Commons: Attribution (CC BY)

*Document Version*

Publisher's PDF, also known as Version of record

*Citation for published version (Harvard):*

Barenghi, CF, McClintock, PVE & Muirhead, CM 2023, 'Vinen's Energy Barrier', *Journal of Low Temperature Physics*, vol. 212, no. 5-6, pp. 185-213. <https://doi.org/10.1007/s10909-023-02945-7>

[Link to publication on Research at Birmingham portal](#)

### General rights

Unless a licence is specified above, all rights (including copyright and moral rights) in this document are retained by the authors and/or the copyright holders. The express permission of the copyright holder must be obtained for any use of this material other than for purposes permitted by law.

- Users may freely distribute the URL that is used to identify this publication.
- Users may download and/or print one copy of the publication from the University of Birmingham research portal for the purpose of private study or non-commercial research.
- User may use extracts from the document in line with the concept of 'fair dealing' under the Copyright, Designs and Patents Act 1988 (?)
- Users may not further distribute the material nor use it for the purposes of commercial gain.

Where a licence is displayed above, please note the terms and conditions of the licence govern your use of this document.

When citing, please reference the published version.

### Take down policy

While the University of Birmingham exercises care and attention in making items available there are rare occasions when an item has been uploaded in error or has been deemed to be commercially or otherwise sensitive.

If you believe that this is the case for this document, please contact [UBIRA@lists.bham.ac.uk](mailto:UBIRA@lists.bham.ac.uk) providing details and we will remove access to the work immediately and investigate.



# Vinen's Energy Barrier

C. F. Barenghi<sup>1</sup> · P. V. E. McClintock<sup>2</sup> · C. M. Muirhead<sup>3</sup>

Received: 22 December 2022 / Accepted: 20 January 2023 / Published online: 13 February 2023  
© The Author(s) 2023

## Abstract

In 1963, the late W. F. (“Joe”) Vinen concluded, partly on intuitive grounds, that the ab initio creation of a quantized vortex line in superfluid  $^4\text{He}$  is impeded by an energy barrier. We place this prescient insight into context and review subsequent theoretical and experimental research that calculated the height of the barrier and validated the result through measurements on negative ions moving through superfluid  $^4\text{He}$  above the Landau critical velocity. We discuss the implications of these results for other superfluids, including laser-cooled dilute atomic gases, and for the subsequent development of superfluid hydrodynamics.

**Keywords** Superfluid · Quantized vortex · Energy barrier · Macroscopic quantum tunnelling · Computer modelling

## 1 Introduction

When the superfluidity of  $^4\text{He}$  was discovered [1, 2] in 1938, it quickly became apparent that the phenomenon only persists while the liquid is being treated “gently”. Thus, the viscous drag on a moving object in the superfluid, or the viscous dissipation in flow through a tube, only remains zero provided that some critical velocity is not being exceeded. The magnitude of the critical velocity varies widely, depending on the experimental geometry and conditions [3, 4].

---

✉ P. V. E. McClintock  
p.v.e.mcclintock@lancaster.ac.uk  
C. F. Barenghi  
carlo.barenghi@newcastle.ac.uk  
C. M. Muirhead  
c.m.muirhead@bham.ac.uk

<sup>1</sup> School of Mathematics, Statistics and Physics, Newcastle University, Newcastle upon Tyne, Tyne and Wear NE1 7RU, UK

<sup>2</sup> Department of Physics, Lancaster University, Lancaster, Lancashire LA1 4YB, UK

<sup>3</sup> School of Physics and Astronomy, University of Birmingham, Birmingham, West Midlands B15 2TT, UK

Below the superfluid transition at temperature  $T = T_\lambda \simeq 2.17$  K the liquid forms a phase known as He II. It behaves as though it were composed of two distinct, interpenetrating, components: superfluid of density  $\rho_s$  and normal fluid of density  $\rho_n$  [6, 7]. The total density of the liquid  $\rho = \rho_n + \rho_s$ . The normal fluid is viscous, albeit with a very small viscosity, and it carries all the thermal energy of the liquid. The superfluid component has zero viscosity for small velocities, and zero entropy being, in effect, at the absolute zero of temperature. As  $T$  decreases, the superfluid fraction  $\rho_s/\rho$  rises from 0 at  $T_\lambda$  to approach unity below 1 K; correspondingly, the normal fluid fraction  $\rho_n/\rho$  falls from unity at  $T_\lambda$  towards zero below 1 K [8]. Following Landau [9, 10], the liquid at low temperatures can be perceived as an inviscid “background” (superfluid component) containing a dilute gas of thermal excitations, phonons and rotons, forming the normal fluid component. Note that the phonons are similar to those in crystals, described at long wavelengths (compared to the average interatomic separation) by a linear dispersion  $\epsilon = cp$  where  $\epsilon$  is the phonon energy,  $p$  its momentum and  $c$  the velocity of sound. Although rotons fall on the same continuous Landau dispersion curve as phonons, they are described by a parabolic particle-like dispersion  $\epsilon = \Delta + \frac{(\hbar k - \hbar k_0)^2}{2\mu}$ , as shown near the local minimum in Fig. 1, where  $\Delta$  and  $\hbar k_0$  are, respectively, the roton energy and momentum at the minimum and  $\mu$  is the roton effective mass. The physical nature of the roton remains an enigma.

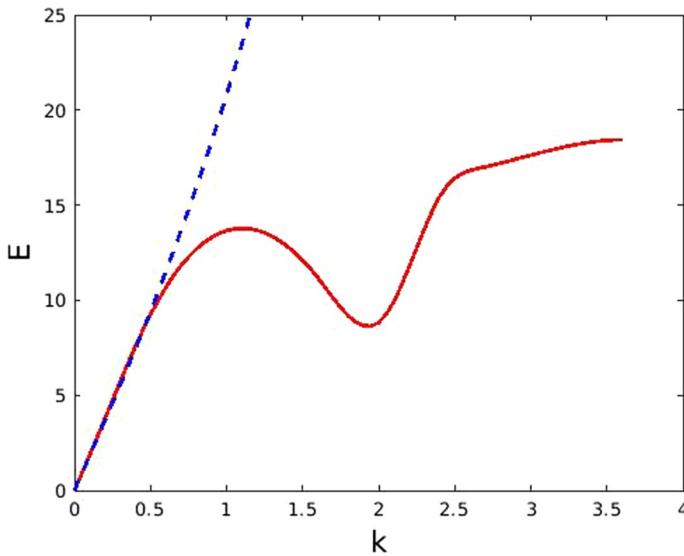


**Fig. 1** Energy–wavenumber dispersion relations for elementary excitations in He II. The energy  $E$  is in units of K and the wavenumber  $k$  is in  $\text{\AA}^{-1}$ . The momentum of an excitation is  $\hbar k$ . The full curve is the Landau spectrum based on the data tabulated by Donnelly et al. [5]. The linear part near the origin corresponds to the phonon regime ( $E \propto p$ ), and the parabolic free-particle-like regime near the local minimum corresponds to rotons. At the roton minimum,  $E/k_B = \Delta$  and  $k = k_0$ . The dashed line represents the GPE dispersion relation (see Sect. 5): it coincides with the Landau spectrum in the phonon regime, but then curves upwards in a free-particle-like regime ( $E \propto p^2$ ) at large  $p$ , without exhibiting a roton minimum

Landau showed that for the kinetic energy of a heavy moving object to be converted directly to heat, i.e., by creation of an excitation of energy  $\epsilon$  and momentum  $p$ , its velocity must exceed  $\epsilon/p$  in order to satisfy conservation of energy and momentum. This argument led naturally to the Landau critical velocity  $v_L = (\epsilon/p)_{\min} \simeq \Delta/p_0$  where  $\Delta$  and  $p_0$  are, respectively, the energy and momentum at the roton minimum in the dispersion curve. At around  $50 \text{ ms}^{-1}$ , depending on pressure,  $v_L$  has been observed [11, 12] and measured [13] under special conditions. The puzzle was that  $v_L$  is much higher than the critical velocities of  $\text{cm s}^{-1}$  or  $\text{mm s}^{-1}$  typically found in experiments. As we discuss in more detail below, the reason for the lower critical velocities usually seen in practice is that dissipation in the superfluid is more commonly associated with quantized vortices.

The superfluid component can be described by a macroscopic wavefunction  $\psi$  [14, 15], related to imperfect Bose–Einstein condensation (BEC) in the liquid for which, even in the  $T \rightarrow 0$  limit, the atomic condensate fraction is only  $\sim 0.1$  [16] (cf.  $\rho_s/\rho \rightarrow 1$  in this limit). Despite the small condensate fraction, liquid  $^4\text{He}$  exhibits a range of macroscopic quantum phenomena closely analogous to those that arise in superconductors [7, 17], in the more-recently discovered BECs formed by laser-cooled gases [18] including roton modes in dipolar quantum gases [19] and among quasiparticles in solids including magnons, excitons and polaritons [20].

For He II, the most dramatic quantum effect is arguably the quantization of the circulation [14, 15, 21], which is given by

$$\oint \mathbf{v}_s \cdot d\mathbf{l} = n\kappa, \quad (1)$$

where  $\mathbf{v}_s$  is the superfluid velocity,  $n = 0, 1, 2, 3, \dots$  is the winding number and the quantum of circulation  $\kappa = h/m_4$ . Here,  $h$  is Planck's constant and  $m_4$  is the  $^4\text{He}$  atomic mass. Eq. (1) means that the superfluid does not rotate, at least not in a simple manner, but remains at rest relative to the fixed stars. If held within a rotating container (one whose geometry is simply-connected), superfluid either does not rotate at all, or one or more quantized vortex lines may appear parallel to the axis of rotation; the exception is superfluid  $^3\text{He-B}$  where, on account of the very high vortex nucleation threshold, a vortex-free region can coexist with a cluster of vortex lines [22]. Since vortex lines with winding numbers larger than 1 are unstable, hereafter we take  $n = 1$ . Each vortex line consists of a core of atomic dimensions around which the tangential superflow velocity falls off inversely with radial distance  $r$  from the center of the core,  $v_s \propto 1/r$ . Vortex rings [23], or closed loops of any shape where a vortex line is joined back on itself, are also possible. Because each element of a ring exists within the net superfluid flow field of the rest of the ring, the ring has an intrinsic translational velocity that is inversely proportional to its radius.

In practice, it is usually vortex lines or rings that are responsible for the breakdown of superfluidity, rather than creation of thermal excitations via the Landau mechanism. However, the dissipation is almost always due to the expansion of existing vortices rather than to their creation ab initio (intrinsic vortex nucleation). Although the critical velocity for intrinsic vortex nucleation has been calculated [24] and measured experimentally [25] (see also Sects. 3 and 4 below), it turns out to be

very high ( $\approx 60 \text{ m s}^{-1}$ ) making the process correspondingly uncommon. Expansion of pre-existing vortices occurs much more easily, at far lower velocities both in  $^4\text{He}$  [3] and  $^3\text{He}$  [26].

In reality, almost all samples of He II, however prepared, seem to contain a few vortices [27] with their ends pinned on the container walls or on solid objects within the superfluid. It is these *remanent vortices* that in practice are usually involved in the breakdown of superfluidity [28]. In what follows we will mainly be concerned, instead, with the physics of the intrinsic mechanisms underlying the breakdown, which in some ways are more interesting and fundamental.

Almost the only way of investigating the breakdown of superfluidity without complications due to remanent vortices is to probe the liquid with ions [29, 30]. These consist of semi-macroscopic charged spheres that may be manipulated with electric fields and detected by the currents they induce in electrodes. The positive ion consists of a  $\text{He}^+$  surrounded by solid helium held by electrostriction, with a radius of  $\approx 0.6 \text{ nm}$ . The normal negative ion is an electron within an otherwise empty bubble, of radius between  $\approx 1.15 \text{ nm}$  (near the melting pressure) and  $\approx 1.7 \text{ nm}$  (under the vapor pressure). Both ions create charged vortex rings when moving under electric fields in He II at low temperatures [23] but the negative ion has the special property that, in He II under pressure, it can reach  $v_L$  without necessarily creating a vortex ring [11, 31], enabling the vortex creation mechanism to be studied (because the probability of an object as small as an ion interacting with the remanent vortex line present in the helium sample is negligible). There are also the elusive fast and exotic negative ions [30] whose properties appear to make them very suitable for studies of vortex creation, but they seem to be difficult to utilize for this purpose in practice, and their structures remain an enigma. The normal negative ion is much more tractable. It has a hydrodynamic effective mass ranging from  $243m_4$  (vapor pressure) [32, 33] down to  $87m_4$  (melting pressure) [34].

In Sect. 2, we review Vinen's argument for there being an energy barrier impeding vortex creation in the superfluid. We discuss how this can be calculated in Sect. 3 and in Sect. 4 we describe experimental measurements of the barrier height. In Sect. 5, we discuss the likely relevance of Vinen's energy barrier to other superfluids. We summarize and draw conclusions in Sect. 6.

## 2 An Energy Barrier Impeding Vortex Creation

At a summer school in 1963, the late W. F. ("Joe") Vinen made what turned out to be a highly prescient remark about the origins of quantized vortices in superfluid  $^4\text{He}$ : that exceeding a critical velocity was a necessary, *but not sufficient*, condition for vortex creation. Based on approximate calculations and physical intuition, he reasoned that there must be an energy barrier impeding the process [35], and he pointed out the need to take this barrier properly into account. His discussion relates to the superfluid and thus, in effect, to the interpretation of flow experiments at very low  $T$  where the normal fluid component can be ignored.

Vinen first estimated the minimum critical velocity  $v_c = (\epsilon/p)_{\min}$  for creation of a vortex ring of radius  $R$  in a two-dimensional flow channel of width  $d$ . Utilizing the

classical expressions for the energy and impulse of a vortex ring [36] and, assuming that the maximum size of the ring will be of order  $d$ , he showed [35] that there is a minimum critical velocity

$$v_c = \frac{\hbar}{m_4 R} \left( \ln \left[ \frac{8d}{a_0} \right] - \frac{7}{4} \right), \quad (2)$$

where  $a_0$  is the vortex core radius. Thus, the critical velocity should decrease with the increasing size of ring created and hence with increasing channel radius. Although this dependence agreed with flow experiments, and although the estimated magnitude of the critical velocity was of the right order, he pointed out that there was a fundamental difficulty.

Even if the relevant critical velocity was being exceeded, so that vortex creation was energetically allowed, there also needed to be an appreciable probability of the process occurring. It must presumably involve a quantum mechanical transition between a state of uniform flow, and a state of flow including the ring. The transition must be induced by interaction with the wall, and therefore accompanied by the excitation of some motion in the wall. It would involve a change in the wave function over a large volume of liquid at a considerable distance from the wall, perhaps  $3 \times 10^{-2}$  cm to match typical experiments. Such a process seemed inherently improbable.

Vinen emphasized that the problem cannot be resolved simply by postulating the initial formation of a very small ring, for which the quantum transition would be less improbable, because even the creation of a small ring involves an increase (not a decrease) in the energy of the liquid and the critical velocity would also be higher. In effect, therefore, there is a large potential barrier opposing the creation of vortex line.

Feynman wavefunctions proved inadequate as a basis for calculating the largest vortex ring whose probability of creation is appreciable but, in any case, the creation of a ring of dimensions much larger than the interatomic spacing seemed intuitively implausible. Vinen also considered the influence of finite temperature and concluded that the thermal excitation of vortices can probably be ignored at low  $T$ , except perhaps near sharp protuberances in the channel walls. Such protuberances would reduce the critical velocity, but not to values as low as those seen in experiments.

Vinen concluded that, because the breakdown of superfluidity normally happens at velocities of the order of  $\text{cm s}^{-1}$  or  $\text{mm s}^{-1}$ , well below the expected critical velocities for vortex creation, the process must usually be seeded by a few lengths of vortex held metastably in the channel, i.e., the remanent vortices discussed above in Sect. 1. It is a picture that has not changed to this day. An important consequence of the presence of remanent vortices is the inherent difficulty of studying the intrinsic breakdown process, a problem to which we return below in Sect. 4.

### 3 Calculation of the Barrier for Negative Ions

Here, we deal only with negative ions (cf. the paper by Muirhead, Vinen and Donnelly (MVD) [24] that also deals with positive ions). We assume that the ions are ideal; smooth, remain spherical under acceleration and are initially vortex free.

We assume that the velocity field due to motion of the vortex-free ion is strictly dipolar (i.e., we ignore any distorting Bernoulli forces and possible complications due to the formation of a virtual roton cloud at the surface of the ion when the local velocity exceeds the Landau critical velocity). We use computer modelling to calculate the minimum velocity at which a vortex can be created at constant impulse and the associated energy barrier to vortex creation. Two possible geometries of vortex nucleation are considered, as shown in Fig. 2: the encircling vortex ring and the attached vortex loop.

For conceptual (and computational) purposes, we note the close analogy between the motion of an (effectively) incompressible fluid ( $\nabla \cdot \mathbf{v} = 0$ ) and that of magnetic fields ( $\nabla \cdot \mathbf{B} = 0$ ):

$$\omega \equiv \mu_0 J; \quad \kappa \equiv \mu_0 i; \quad v \equiv B; \quad (3)$$

where  $J$  is the current density,  $i$  is the total current,  $B$  is the resulting magnetic field,  $\omega$  is the vorticity,  $\kappa$  is the circulation and  $v$  is the local fluid velocity. Schwarz and Jang stated [37], and Vinen showed more explicitly, that the total momentum (more accurately the impulse) of the ion/vortex complex fluid, and the total kinetic energy, are given by

$$P_c(U) = P_c(0) + P_0(U), \quad (4)$$

$$E_c(U) = E_c(0) + E_0(U), \quad (5)$$

where  $P_c(U)$  and  $E_c(U)$  are the impulse and energy of the ion-vortex complex at ion velocity  $U$ ;  $P_0(U)$  and  $E_0(U)$  refer to the free ion, i.e., in the absence of any vorticity. This is a considerable simplification from the computational viewpoint. The ion

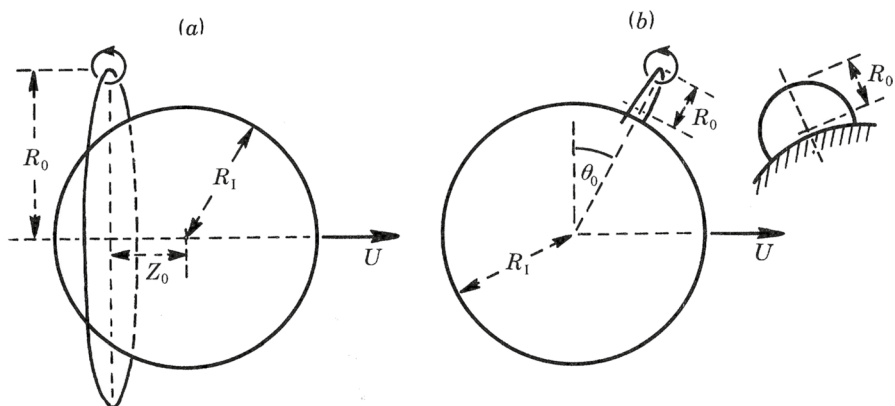


**Fig. 2** Two possible geometries of the nucleating vortex: **a** an encircling ring; **b** an attached loop.  $R_1$  is the radius of the ion;  $R_0$  is the radius of the ring or loop; and  $U$  is the ion's velocity. In **a**,  $Z_0$  is the displacement of the loop from the equatorial plane and, in **b**,  $\theta_0$  is the angle of the loop relative to the equatorial plane. Reprinted figure with permission, from Muirhead et al. [24]. Copyright (1984) by the Royal Society of London

of radius  $R_1$  is virtually empty (see Sect. 1), so it has only the hydrodynamic mass  $M_I = (2/3)\rho_s\pi R_1^3$  giving us for the vortex-free impulse and energy

$$P_0(U) = (2/3)\rho_s\pi R_1^3 U, \quad (6)$$

$$E_0(U) = (1/3)\rho_s\pi R_1^3 U^2, \quad (7)$$

where we have equated the superfluid density and the total density at low temperatures. The computations therefore reduce to the calculation of impulse and energy for the stationary ion in the presence of a vortex loop or ring.

The velocity field due to the vortex is clearly affected by the presence of the fluid-free ion. It may help the reader to consider the magnetostatic analogy, which is that of a current-carrying loop or ring in the presence of a superconducting sphere. In both geometries shown in Fig. 2, current flows on the surface of the sphere and is so distributed that, inside the sphere, the magnetic field is everywhere zero. The problem of calculating the  $\mathbf{B}$  field (fluid velocity) is most easily solved by using the method of images. Here, an imaginary current inside the sphere (the image) is constructed such that it produces a field outside the sphere everywhere the same as that produced by the real currents (on the surface of the sphere) and obeys the boundary condition that magnetic field normal to the surface of the sphere is everywhere zero.

This is most conveniently calculated by considering the vector potential  $\mathbf{A}$  where  $\mathbf{B} = \nabla \times \mathbf{A}$ . We are at liberty to choose the gauge of  $\mathbf{A}$  such that  $\nabla \cdot \mathbf{A} = 0$  without altering the measurable quantity  $\mathbf{B}$ . In this gauge, the vector potential due to a current element  $i\mathbf{dl}$  is given by  $\mathbf{A} = \mu_0 i\mathbf{dl}/(4\pi|r|)$ , exactly analogous to the equation for the scalar potential due to a point charge. The problem of determining the image of a current element  $i\mathbf{dl}$  in a superconducting sphere is then formally equivalent to the well-known problem of determining the image of a charge in a conducting sphere. We simply have to remember to apply this to all vector components of  $i\mathbf{dl}$ . In Fig. 3, we show the two components of  $i\mathbf{dl}$ . The image of a current element in the horizontal direction (Fig. 3b) is of magnitude  $(R_1/z)i\mathbf{dl}$  positioned at a radius  $R_1^2/z$ .

It follows immediately that the image of the Schwarz and Jang vortex ring is a ring of opposite sense, having circulation  $\kappa(R_1/z)$  at the radius shown, irrespective of its displacement along the direction in which the ion moves (see Fig. 2).

In the case of the vortex loop, we need to be a bit more careful. Vinen noted that the radial component shown in Fig. 2a does not require an image, but we may give it one. If we follow the same prescription as used in Fig. 2b, it is easily seen that the image lies on a continuation of the real vortex to produce a (vortex + image) that is a complete circle of radius  $R_0$ . However, the magnitude of the current in the image reduces as we move further from the surface of the ion, so the current in the image is not conserved. This produces a  $\mathbf{B}$  field outside the sphere that does not obey Maxwell's equations and the image must therefore be incomplete.

Vinen realized that you can always add to this image a fan of currents along any radius centered on the sphere (Fig. 4). This is allowed because such currents satisfy the boundary condition  $B_{\text{normal}} = 0$ . The currents flowing in the fan elements are chosen so that current continuity is obeyed and Maxwell's equations are satisfied.



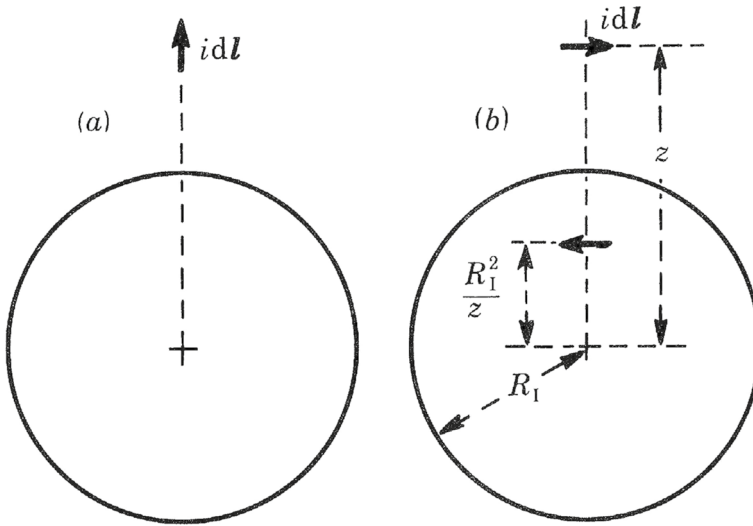
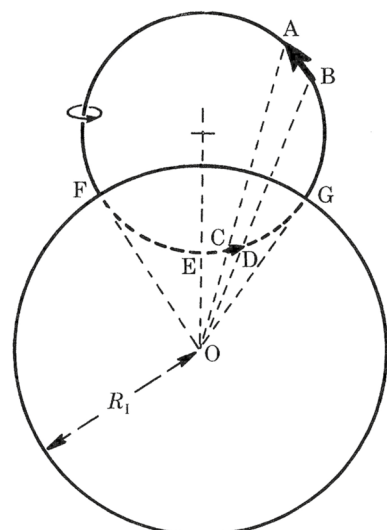


**Fig. 3** Images of current elements in a superconducting sphere. Reprinted figure with permission, from Muirhead et al. [24]. Copyright (1984) by the Royal Society of London

### 3.1 Energy and Impulse

We initially assume that the radius of the vortex core is small compared with all other dimensions. This is clearly not the case for a vortex ring very close to the ion or for a vortex loop as we approach points F and G in Fig. 4. We will find that the energy barrier to vortex formation involves very small vortex loops

**Fig. 4** Image of a vortex loop in a solid sphere. Reprinted figure with permission, from Muirhead et al. [24]. Copyright (1984) by the Royal Society of London



or rings close to the ion, so corrections to the energy and impulse calculations will be important. We outline Vinen's estimates of the necessary corrections in Sect. 3.2.

We return now to the hydrodynamic situation. We first note that the energy due to the vorticity

$$E_c(0) = (1/2)\rho_s \int v^2 d\tau, \quad (8)$$

where the integral is taken over the fluid volume. This can be expressed as

$$E_c(0) = (1/2)\rho_s \int (\mathbf{A} \times \mathbf{v}) \cdot d\mathbf{S}, \quad (9)$$

where  $\mathbf{v} = \nabla \times \mathbf{A}$  and the integral is taken over all surfaces bounded by the fluid (the contribution from the surface at infinity being zero); and  $\mathbf{v}$  is obtained from the hydrodynamic equivalent of the Biot–Savart law in magnetostatics. The computations therefore reduce to the problem of performing an integral over the surface of the ion and the vortex (which we again treat as a circular tube of radius  $a_0$ ). For the stationary ion, there are two contributions to the integral over the vortex: that due to the vortex itself; and that due to the image. The energy of a vortex ring in an unbounded fluid is given [36] by

$$E = \frac{1}{2}\rho_s \kappa^2 R \{\ln(8R/a_0) - 1.62\}, \quad (10)$$

where  $R$  is the radius of the ring. In the case of a vortex loop this must be corrected for the portion of the loop that is missing. We note that the numerical value of 1.62 is dependent on the particular model for the nature of the vortex core, about which little was known at the time of Vinen's paper [35], and which remains to this day something of a conundrum: Table 1 of Ref. [38] lists numerical values of  $\frac{7}{4}$ ,  $2$ ,  $\frac{3}{2}$ , 1.615, and 2.05 corresponding, respectively, to a solid core of constant volume, a hollow core at constant pressure, a hollow core with surface tension, the GPE solution, and a viscous core. The question is hard to resolve experimentally because of the effect of the logarithm. In addition,  $\mathbf{A}$  and  $\mathbf{v}$  at the surface of the vortex core are changed, because the missing part of the complete ring is replaced by the image.

In the case of the encircling ring, it was shown by Schwarz and Jang [37] that the vector potential is zero over the surface of the ion and therefore there is no contribution to the integral from the core surface. For the vortex loop, the vector potential cannot be zero and the contribution from the surface of the ion must be evaluated.

Vinen showed that the impulse at zero ion velocity may be written in the form

$$\mathbf{P}_c(\mathbf{0}) = \frac{1}{2}\rho_s \kappa \int \mathbf{r} \times d\mathbf{l}, \quad (11)$$

where the integral is evaluated over the real vortex and its image.

### 3.2 Corrections for Small Rings

As we have already noted, we expect the dominant energy barrier to vortex formation to involve small radii for vortex loops and rings close to the ion surface and, as we shall see, this is confirmed in the results of our computations in Sect. 3.4 below.

In the MVD paper [24], Vinen exerted considerable effort to make the best reasonable estimates of the corrections, based on the limited information available at the time. These estimates were quite detailed and the interested reader is referred to that paper. We should, however, summarize Vinen's thinking on this issue.

For the case of the vortex loops, Vinen used the best available theoretical calculations of impulse and energy for small rings in an unbounded fluid [36] and fitted them to a mathematical function, which was then scaled according to the size of the vortex loop. For the case of the encircling rings, he took the best available calculations for a pair of rectilinear parallel vortices of opposite strengths, which mimicked the vortex ring and its image. Where the vortex ring was displaced from the ion along the direction of travel, interpolation between the rectilinear vortex pair and small ring was required.

### 3.3 Computational Techniques

For integrals over the surface of the ion, the surface was divided into  $\sim 1000$  elements and, for the vortex ring and its image,  $\sim 500$  straight sections. The size of each element was reduced in regions where the velocity, vector potential or vorticity were changing rapidly with position. As we have already noted, there is no contribution from the surface in the case of the encircling ring. The number of elements was varied and limiting cases were examined in order to determine accuracy within the assumptions and approximations referred to earlier. It was estimated the numerical accuracy was good to  $\sim 0.5\%$ . Programming was conducted in Fortran.

### 3.4 Results of the Computations

The computational results reported in the MVD paper were extensive, covering positive and negative ions, both the vortex loop and encircling ring geometries, and a range of pressures. In keeping with the purpose of the present paper, we will restrict ourselves to a few illustrative examples. In Sects. 3.6 and 3.7, we will consider the problem addressed by Vinen, which is the probable rate at which vortex lines can be generated.

The computed energy changes at constant momentum for negative ions are shown in Fig. 5. We see that the critical velocities for the loop and ring are  $\sim 45 \text{ ms}^{-1}$  and  $\sim 70 \text{ ms}^{-1}$ , respectively. In both cases, there is an energy barrier to vortex formation, but it is much larger for the encircling ring for which the tunnelling distance is larger by more than a factor of 2.

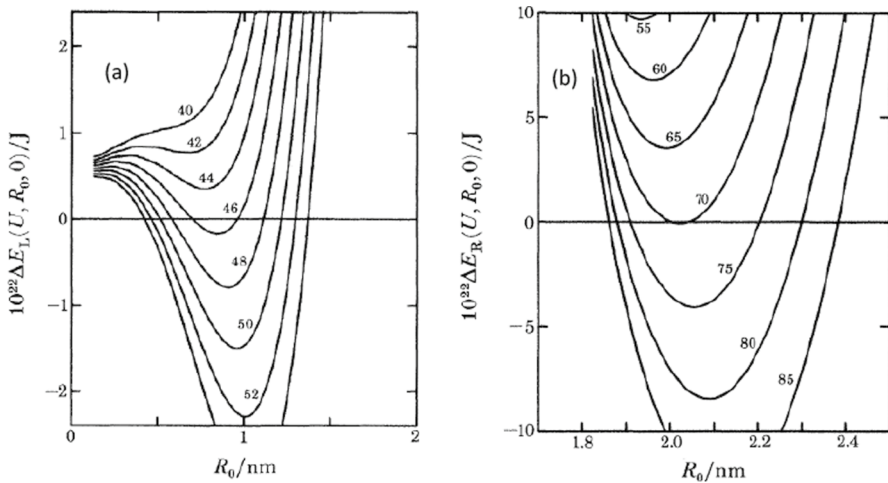


**Fig. 5** Energy change at constant impulse as a function of vortex radius  $R_0$  for negative ions at a pressure of 0 Pa, **a** for a vortex loop, **b** for an encircling ring at the equator. The number against each curve is the value of the initial ion velocity  $U$  in  $\text{m s}^{-1}$ . Reprinted figure with permission, from Muirhead et al. [24]. Copyright (1984) by the Royal Society of London.

### 3.5 Effect of the Nucleating Geometry

So far we have considered vortex loops and rings whose axes lie along the direction of the ion velocity and for rings in the equatorial plane. In Fig. 6, however, we show contours of constant energy for different positions of the loop and of the ring.

Extensive computations over a range of initial velocities show that the minimum critical velocity for vortex loop creation always lies in the equatorial plane. Loops can be created outside the equatorial plane for higher initial velocities (Fig. 6a).

Vortex rings are more complicated. Rings can only be created in the equatorial plane for initial velocities greater than  $\sim 70 \text{ m s}^{-1}$ . At initial velocities comparable with, but still significantly higher than those for vortex loop creation (Fig. 6b), rings can be created out of the equatorial plane, but with energy barriers that are much wider and higher than for vortex loops. This gives strong support for Vinen's view that vortex loops are created at substantially lower initial velocities than for rings.

### 3.6 Vortex Nucleation by Quantum Tunnelling

We confine ourselves to vortex loops. Impeding their formation, there is an energy barrier of height  $\sim 5 \times 10^{-23} \text{ J}$  and width  $\sim 4 \times 10^{-10} \text{ m}$ . Here, we assume that the energy barrier drops near to the ion, where the distance of the vortex from the ion becomes comparable with the vortex core diameter. Vinen argued that this is physically reasonable, because the energy barrier must go to zero for zero loop radius. We now address the question of the tunnelling probability through such a barrier.

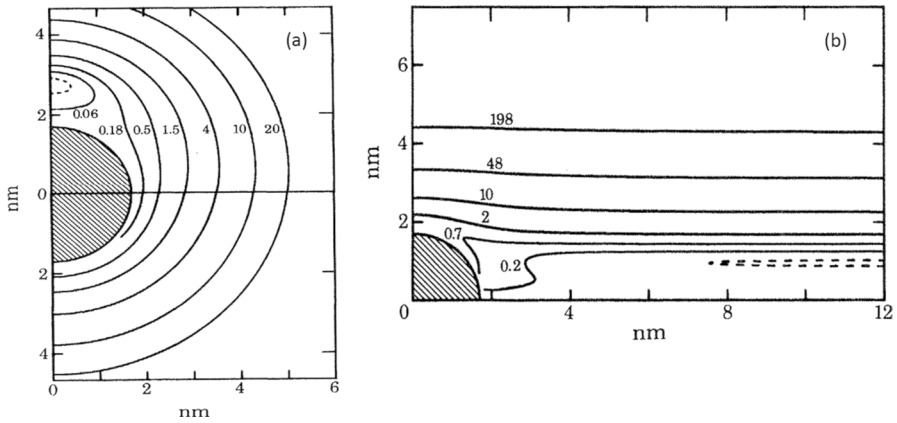


**Fig. 6** Contours of constant energy change at a pressure of 0 Pa and fixed initial velocity: **a** for a vortex loop with initial velocity  $46 \text{ m s}^{-1}$ ; and **b** for a vortex ring with an initial velocity  $72 \text{ m s}^{-1}$ . Each graph is plotted on a plane of symmetry through the center of the ion (shaded) and parallel to the initial ion velocity  $U$ . The size and position are specified by the point at which the vortex crosses this plane. The axes represent the distances from the center of the ion. The number close to each curve is the value of  $10^{21} \Delta E_L / J$  for a loop and  $10^{21} \Delta E_R / J$  for a ring. The broken curves are the contours of  $\Delta E_L = 0$  (loop) and  $\Delta E_R = 0$  (ring). Reprinted figure with permission, from Muirhead et al. [24]. Copyright (1984) by the Royal Society of London

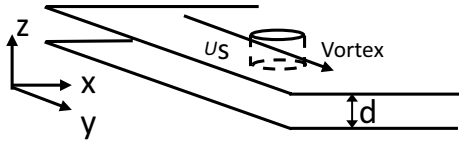
We will see in Fig. 11 (below) that the vortex nucleation rate becomes more or less temperature independent at temperatures below  $\sim 0.6\text{K}$ . This led Vinen to suggest that vortex nucleation at low temperatures was a result of penetration of the energy barrier by quantum tunnelling. Processes of this type had been considered by Volovik [39], Sonin [40] and Ichiyanagi [41] but these authors had failed to take account of the hydrodynamic mass of the core. Our analysis so far implicitly assumes that the vortex has a fluid filled core. We shall see, in this section, that we assume the core is hollow, so that it has a hydrodynamic mass due to the missing fluid. This has little effect on our previous calculations, at least in the limit where the vortex radius is large compared with the core radius. In any case, it is a small logarithmic factor. This can be subsumed into a small change in the core radius which was not well known and is still not well defined.

Vinen noted that “A realistic calculation of the production of vortex loops by quantum tunnelling is difficult, and we do not know how to do it.” Vinen therefore proposed to solve the problem in the simpler geometry of a 2-dimensional sheet of helium and then consider how the results could realistically be carried over into the creation of vortex loops. The calculation is detailed and beyond the scope of the present paper, for which the interested reader is referred to MVD. We will, however, outline the argument drawing attention to key points. The geometry used by Vinen is shown in Fig. 7.

The equation of motion due to the Magnus force on the vortex is

$$m_v \ddot{\mathbf{r}} = \rho_s (\mathbf{v}_s - \dot{\mathbf{r}}) \times \boldsymbol{\kappa}. \tag{12}$$

**Fig. 7** Liquid helium is trapped between two parallel sheets. We assume the vortex is short, straight and far from the boundaries



where  $m_v$  is the hydrodynamic mass which, for a hollow core, is  $m_v \sim \pi \rho_s a_0^2$  per unit length,  $v_s$  is the local velocity field, and  $\kappa$  is the quantum of circulation treated as a vector. We expand this as

$$m_v \ddot{\mathbf{r}} = \rho_s \kappa \mathbf{v}_s \times \hat{\mathbf{k}} - \rho_s \kappa \dot{\mathbf{r}} \times \hat{\mathbf{k}}, \tag{13}$$

This has the same functional form as that of an electrostatic line charge ( $q$  per unit length) attached to a line mass ( $m$  per unit length) moving in a direction perpendicular to its length in an electromagnetic field ( $E, B$ )

$$m_v \ddot{\mathbf{r}} = q\mathbf{E} + q\dot{\mathbf{r}} \times \mathbf{B}. \tag{14}$$

Our analogy is therefore

$$q \equiv \kappa, \mathbf{E} \equiv \rho_s \mathbf{v}_s \times \hat{\mathbf{k}}, \mathbf{B} \equiv -\rho_s \hat{\mathbf{k}}. \tag{15}$$

We now assume a Cartesian co-ordinate system. In the special case where  $E$  is in the  $x$ -direction and  $B$  and the line charge are in the  $z$  direction, the motion of the line charge is a drift velocity  $E/B$  in the  $y$ -direction superimposed on a cyclotron motion about a line parallel to, but displaced from, the line charge by the cyclotron radius. Its instantaneous potential energy is  $E(x - b)$ , where we have taken the potential energy as zero at  $x = b$ .

For the case of the vortex, we take the local velocity field to be  $U_s$  in the  $y$ -direction. It follows from our analogy that, in the geometry shown in Fig. 7, the vortex motion will be a cyclotron motion in the  $x - y$  plane with a drift velocity  $U_s$  in the  $y$ -direction. The potential energy of the vortex is  $\rho_s \kappa d U_s (x - b)$ . The quantum mechanical wave equation is therefore

$$\frac{\partial^2 \psi}{\partial x^2} + \left( \frac{\partial}{\partial y} + \frac{i \rho_s \kappa d x}{\hbar} \right)^2 \psi + \frac{2m_v d}{\hbar^2} \{ \epsilon + \rho_s \kappa d U_s (x - b) \} \psi = 0, \tag{16}$$

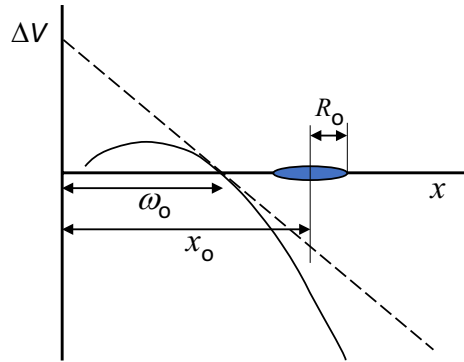
where we have used a gauge for the vector potential equivalent in the magnetic case to  $(0, Bx, 0)$ . To solve Eq. (16), we first make the substitution

$$\psi = e^{ik_y y} u(x). \tag{17}$$

Following a lengthy but straightforward derivation and the use of the WKB approximation, we obtain

$$u_n(x) \sim \exp \left[ \frac{-\rho_s \kappa d}{\hbar} \int_{x_0 \pm r_0}^x \{ (x_0 - x)^2 - r_0^2 \}^{1/2} dx \right], \tag{18}$$

**Fig. 8** A schematic of the potential barrier impeding the formation of a vortex. The solid line represents Eq. (19) and the dashed line is an approximation representing Eq. (20)



where the eigenfunctions are centered on  $x_0$  and the cyclotron radius is  $r_0$ . The eigenfunctions turn out to be those of a harmonic oscillator with energy index  $n$ . Only the value  $n = 0$  gives significant tunnelling probability.

We consider the nucleation of a vortex at the edge of a thin film due to quantum tunnelling. The tunnelling barrier is given by

$$\Delta V = \frac{\rho_s \kappa^2 d}{4\pi} \ln \left( \frac{2x}{a_0} \right) - \rho_s \kappa dx U_s. \tag{19}$$

The first term is due to the interaction of the vortex with its image: the second term is from its interaction with the velocity field  $U_s$ . This is shown schematically in Fig. 8.

In order to make the derivation more tractable, the barrier is replaced by the dashed line

$$\Delta V = \rho_s \kappa d U'_s (\omega_0 - x), \tag{20}$$

where  $U'_s$  is around half  $U_s$ . We assume that the film is formed between two smooth surfaces and is bounded at  $x = 0$  by a wall in the  $y - z$  plane (see Fig. 7). The vortex is formed by an interaction between this wall and the helium, involving an exchange of momentum between the wall and the helium. This can only occur if the surface is rough.

We consider first a single protuberance leading to a perturbation  $V$  in the helium. Ideally, we would calculate a tunnelling rate given by

$$\nu_0 = \frac{2\pi}{\hbar} \left| \int \psi_f^* V \psi_i d\tau \right|^2 g(\epsilon), \tag{21}$$

where  $\psi_i$  is the initial (vortex free) state,  $\psi_f$  is the final (with vortex) state, and  $g(\epsilon)$  is the final density of states associated with the vortex. Unfortunately  $V$  is not known so Vinen took a different approach. He first reasoned that in the absence of the potential barrier, the frequency with which vortices were created was the frequency with which the vortex would interact with the protuberance, i.e., the cyclotron frequency ( $\rho_s \kappa / m_v$ ), which is very large ( $\sim 10^{13}$  Hz). This rate would be reduced by a

factor of order the extent to which the wavefunction of the vortex in its final state overlapped the perturbing protuberance in the wall. He found

$$v_0 \sim \frac{\rho_s \kappa}{m} \exp \left\{ -\frac{\rho_s \kappa d}{\hbar} \left( w_0 + \frac{\hbar}{2m_v d U'_s} \right)^2 \right\}. \quad (22)$$

In order to approximate this to the case of the ion, we replace  $w_0$  by our computed barrier width, put  $d$  equal to the length of a loop at the point of tunnelling (roughly  $\pi w_0$ ) and the prefactor to be the cyclotron frequency multiplied by the number of atoms on the surface of the ion. We note that Eq. (17) implies that, in the case of the 2-dimensional sheet, the vortex is delocalized in the  $y$ -direction, so in the ion case, is delocalized in the azimuthal plane. The assumption that the protuberances involve all atoms on the ion surface is therefore not unreasonable.

This procedure was found to give quite good agreement with experimental data for the critical velocity [42].

There is, however, a feature of the experimental results that Vinen's theory does not correctly predict: at higher velocities the vortex nucleation rate actually drops. Our computations do not support the explanation proposed by Bowley et al. [42], that this is due to escape from nascent vortex rings, so Vinen proposed quite a different explanation. It had been widely assumed that vortex creation and the generation of rotons (intrinsic to the experiments of McClintock et al.) could be treated as independent processes.

Roton generation, however, constitutes a form of scattering and hence a frictional force. The effect of friction on quantum tunnelling was considered by Caldeira and Leggett [43]. They found that in the presence of friction, the tunnelling rate is reduced by a factor

$$e^{-A\eta\Delta q^2/\hbar}, \quad (23)$$

where  $\eta$  is the friction coefficient,  $\Delta q$  is the barrier width and  $A$  is a constant of order unity. Applying this to a vortex loop and using the substitutions above we get a factor

$$e^{-Amdw_0^2/\hbar\tau}, \quad (24)$$

where  $\tau$  is the relaxation time, which we identify with the inverse rate of emission of roton pairs.

The data of Bowley et al. [42] at a pressure of  $1.7 \times 10^6$  Pa shows a fall-off in nucleation rate for fields greater than  $7.5 \times 10^5$  V/m, which implies a nucleation rate for vortex pairs of about  $2.7 \times 10^{10}$  s<sup>-1</sup>. Using our previous parameters and  $w_o = 3 \times 10^{-10}$  m we find that the above exponential is  $\exp(-0.27)$ . Given the uncertainty in  $A$  and the crudeness of our model, it is not unreasonable to assume that the fall in vortex creation rate is depressed by roton emission and therefore that the processes of roton emission and vortex creation should not be taken as entirely independent.

Vinen was very clear that the whole of this quantum tunnelling theory was approximate and tentative. He stated in the conclusion that "Our own discussion of



this effect is speculative and possibly wrong”. It is a testament to his intuition and analytic skills that so much of it has stood the test of time.

### 3.7 Vortex Nucleation by Thermal Excitation

The main thrust of (MVD) was the creation of a vortex by quantum tunnelling at zero Kelvin. At finite temperature, however, nucleation of a vortex by thermal activation becomes possible. As we will see in Fig. 11, there is a sharp rise in nucleation rate at temperatures above  $\sim 200$  mK. The height of the potential barrier against vortex nucleation is typically  $5 \times 10^{-23}$  J, corresponding to a temperature of  $\sim 3.6$  K. Thermal activation over this barrier requires only a single roton or phonon and, due to the nature of the dispersion curve, the roton density greatly exceeds that of phonons except at the lowest temperatures. The roton density falls exponentially with temperature, however, and below  $\sim 200$  mK it becomes negligible. The nucleation of vortex loops by thermal activation had been considered [44] by Donnelly and Roberts in 1971, but without proper consideration of energy and momentum conservation. Thermal activation by absorption of a roton, taking these conservation conditions into account, was dealt with by Bowley et al. [42] and thermal activation by phonons at the lower temperatures was investigated by Hendry et al. [25].

## 4 Experiments to Measure the Barrier

In order to investigate the ab initio creation of quantized vortices in He II one would like, ideally, to monitor vortex-free superfluid flowing at a constant, controlled velocity or, alternatively—in line with the theory presented in Sect. 3—to study the dynamics of a negative ion moving through the superfluid at a constant velocity. The small size of the ion means that, even though the superfluid contains a small density of remanent vortices, their influence can be ignored because it is most unlikely that the ion will encounter any of them.

### 4.1 Controlling the Ionic Velocity at Low $T$

To move an object through superfluid with constant velocity at very low temperature is a challenging problem, because the smallest force will cause it to accelerate continuously and because of heating where mechanical actuators are used. Nonetheless, methods have been developed to pull a grid at constant velocity with minimal heat generation [45] and to move wires or grids at constant speed in arcs of circle [46, 47]; very recently, a technique has been proposed [48] that would enable a levitated macroscopic object to be moved at constant velocity in a short straight line, or perpetually in circular motion at constant speed, but its successful realization has yet to be reported.

In the case of ions, small stray electric fields will cause continuous acceleration. The simple method of controlling the ionic velocity used here involved balancing the force on the ion from an applied electric field against the rate of momentum loss associated

with roton creation at velocities above the Landau critical velocity  $v_L$ . The applied fields were much stronger than any stray fields, so the influence of the latter could be ignored. The variation of the ionic velocity with time is believed to take the form of a sawtooth [12]: the ion accelerates freely until it becomes energetically possible to emit a pair of rotons [31]; in doing so, its velocity decreases discontinuously due to its small effective mass; after which it accelerates again. The sawtooth shape is unobservable in practice because the contribution from a single ion is too small, and the stochastic roton emission processes are not synchronized for different ions in the ensemble. The whole sawtooth rises in average velocity with increasing electric field. It is assumed that roton creation and vortex nucleation are independent processes and that the most likely circumstance for vortex nucleation will be when the ion is at its maximum velocity, because of the decreased barrier height (see Fig. 5). At one of the sawtooth maxima, therefore, the ion is expected to generate a vortex loop rather than emitting a pair of rotons.

For the method to work, the critical velocity  $v_V$  for vortex creation must obviously be higher than  $v_L$ . Fortunately, this condition can readily be met by adjustment of the ambient pressure  $P$ :  $v_L$  falls with increasing  $P$  [13], whereas  $v_V$  increases [42]. It is also necessary to use isotopically purified  $^4\text{He}$ , because tiny quantities of  $^3\text{He}$  exert a dramatic influence on the vortex creation process, reducing the critical velocity and simultaneously increasing the probability of vortex creation [49].

## 4.2 Measurement of the Vortex Nucleation Rate

The rate  $\nu$  at which negative ions nucleate vortices can be measured by use of the electric induction method described in detail by Bowley et al. [42]. Briefly, a disk-shaped ensemble of ions is propagated in a strong electric field between a pair of parallel electrodes whose diameter is much larger than their separation and than the diameter of the ion disk, as sketched in Fig. 9. If there were no vortex nucleation, a constant current would be induced in the collecting electrode towards which the ions are moving, which is held at fixed potential. When an ion nucleates a vortex, however, the resultant charged ring grows very rapidly and correspondingly slows down abruptly. The charge effectively stops, almost instantaneously, and it therefore ceases contributing to the induction current in the collector. The measured current therefore takes the form of a decaying exponential  $\propto e^{-\nu t}$ , enabling  $\nu$  to be measured. A typical induction signal is shown in Fig. 10.

## 4.3 Experimental Results

Some measurements of  $\nu$  made in this way are shown in Fig. 11 as a function of reciprocal temperature  $T^{-1}$ . There is evidently a temperature-independent regime below  $\sim 100$  mK and a rapid rise in  $\nu$  above  $\sim 200$  mK. The data can be fitted to a relation of the form

$$\nu = \nu(0) + Ae^{-\epsilon/k_B T}, \quad (25)$$

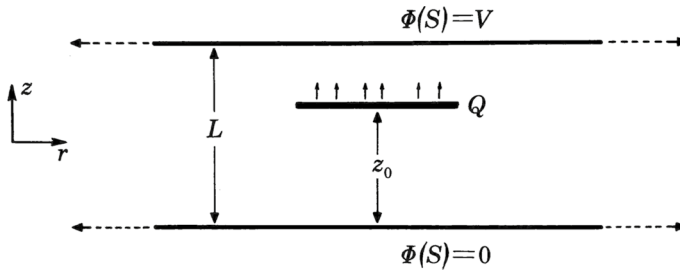


**Fig. 9** Idealized cell geometry for measuring the vortex nucleation rate  $\nu$  by electric induction [42]. An infinitesimally thin disk-shaped ensemble of bare ions, total charge  $Q$ , is driven at constant velocity from the lower plate at potential  $\Phi(S) = 0$  towards the upper one at potential  $\Phi(S) = V$  by a uniform electric field. If there is no vortex nucleation between the plates, a constant current will flow from the upper plate in order that its potential should remain equal to  $V$ . If nucleation is occurring at rate  $\nu$ , however, the current will be proportional to  $e^{-\nu t}$ , where  $t$  is time. Reprinted figure with permission, from Bowley et al. [42]. Copyright (1982) by the Royal Society of London

where  $\nu(0)$  represents the temperature-independent value of  $\nu$  in the low  $T$  limit, and  $A$  and  $\epsilon$  are constants. In the light of the theory and discussions of Sects. 2 and 3, it is natural to identify  $\nu(0)$  with quantum tunnelling through Vinen's energy barrier and the second term in Eq. 25 with thermal activation over the barrier, of height  $\epsilon$ . Figure 12 compares relevant results from Sect. 3 with the barrier height  $\epsilon$  from the measurements. The agreement is excellent and, in fact, better than expected given that the calculated height is an estimate with an uncertainty of up to a factor of  $\sim 2$ .

Taken with the MVD calculations [24] described in Sect. 3, these results constitute a convincing vindication of Vinen's inferred energy barrier [35] impeding the nucleation of vortices in superfluid  $^4\text{He}$ . It is interesting to consider whether or not similar barriers to vortex nucleation occur in other superfluids.

## 5 Further Developments

### 5.1 The Gross–Pitaevskii Equation

Although the MVD calculations [24] and the experiments [12] which we have described settled the main physics issue, a fundamental problem still remains: in the MVD scenario, what creates the “proto-vortex” (the encircling ring or the attached loop), which, in the presence of a superflow, may or may not expand and become observable?

The MVD approach is semi-classical: it is based on the theory of inviscid fluids, neglects density variations (waves) and assumes that the core of the quantum vortex is much smaller than any other length scales of the problem. The MVD paper relies primarily on the latter assumption. Vinen made use of considerable intuition to derive and justify modifications to the computations when this approximation is no longer applicable (see Sect. 3.2). However, the radius of the negative ion,  $a \approx 1$  nm, is larger, but not much larger than the radius of the vortex core,  $a_0 \approx 0.1$  nm, and the

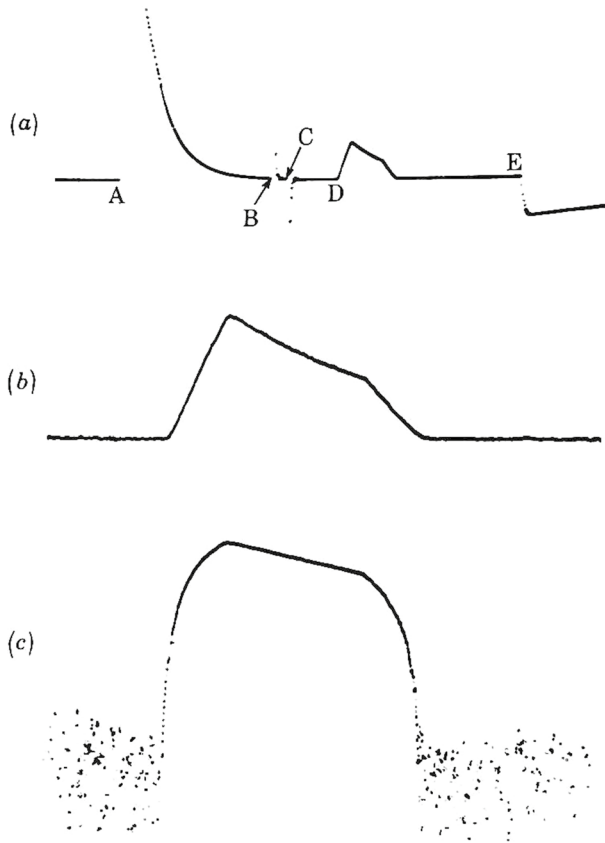


**Fig. 10** Typical signal recorded at the collector [42] under a pressure of  $P = 17$  bar. **a** Measured signal as a function of time. The actual induction signal starts at D corresponding to the moment when the front of the charge disk first enters the induction space; the finite rise-time corresponds to the finite thickness of the charge disk, unlike the idealized disk shown in Fig. 9. The transients that occur at A, B, C and E, overloading the signal pre-amplifier, relate to the operation of the field emission source and the gating of the charge to create the disk. **b** Enlarged version of the induction signal in **a**. **c** Logarithm of the signal shown in **b**. It has a linear top, demonstrating the exponential decay of the signal. Reprinted figure with permission, from Bowley et al. [42]. Copyright (1982) by the Royal Society of London

critical velocity of vortex nucleation,  $v_c \approx 60\text{s}^{-1}$ , is smaller, but not much smaller than the speed of sound in  $^4\text{He}$ ,  $c \approx 238$  m/s. The condensate model which we summarize below provides an alternative approach which avoids the MVD approximations of infinitesimal vortex core thickness and incompressibility.

In the mean field approximation, the macroscopic complex wavefunction  $\psi(\mathbf{x}, t)$  of a condensate of  $N$  bosons of mass  $m$  which weakly interact via the potential  $U$  obeys the equation

$$i\hbar \frac{\partial \psi}{\partial t} = -\frac{\hbar^2}{2m} \nabla^2 \psi + \psi \int |\psi(\mathbf{x}', t)|^2 U(|\mathbf{x} - \mathbf{x}'|) d\mathbf{x}' + V\psi - \mu\psi, \quad (26)$$

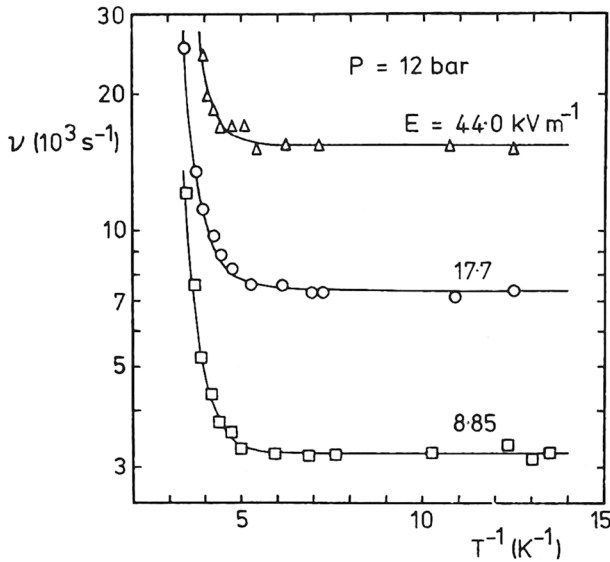


**Fig. 11** The vortex nucleation rate measured for negative ions in isotopically pure He II, plotted as a function of reciprocal temperature  $T^{-1}$  for three electric fields  $E$  [50]. The curves represent fits of Eq. (25) to the experimental data (points). Reprinted figure with permission, from Hendry et al. [50]. Copyright (1988) by the American Physical Society

where  $\mu$  is the chemical potential and the normalization of the wavefunction is

$$N = \int |\psi(\mathbf{x}', t)|^2 d^3 \mathbf{x}'. \tag{27}$$

The potential  $V(\mathbf{x}, t)$  is imposed externally to confine the gas or to model a moving ion. Assuming repulsive contact interactions between pairs of bosons, the potential  $U$  becomes a delta function of strength  $g > 0$ , and Eq. 26 reduces to the Gross–Pitaevskii equation (GPE):

$$i\hbar \frac{\partial \psi}{\partial t} = -\frac{\hbar^2}{2m_4} \nabla^2 \psi + g|\psi|^2 \psi + V\psi - \mu\psi. \tag{28}$$

A property of the GPE which is particularly important in the vortex nucleation problem is that it conserves both energy and momentum. Using the Madelung transformation  $\psi(\mathbf{x}, t) = \sqrt{n(\mathbf{x}, t)}e^{iS(\mathbf{x}, t)}$ , where  $S(\mathbf{x}, t)$  is the phase of  $\psi$ , the condensate can be described as a fluid [51] of velocity  $\mathbf{v}(\mathbf{x}, t) = (\hbar/m_4)\nabla S(\mathbf{x}, t)$  and density  $\rho(\mathbf{x}, t) = m_4 n(\mathbf{x}, t)$  where  $n(\mathbf{x}, t) = |\psi(\mathbf{x}, t)|^2$  is the number of atoms per unit volume. The fluid’s pressure consists of two parts: an ordinary barotropic pressure  $gn^2/2$ , and a so-called quantum pressure which is proportional to  $\hbar^2$  (hence vanishes in the classical limit  $\hbar \rightarrow 0$ ).

A quantum vortex is a solution of the GPE such that  $\psi = 0$  along a line around which the phase changes by  $2\pi$ . In this way Eq. 1 is satisfied. The line (the vortex axis) is surrounded by a tubular region of depleted density of radius  $a_0 \approx \xi$  where

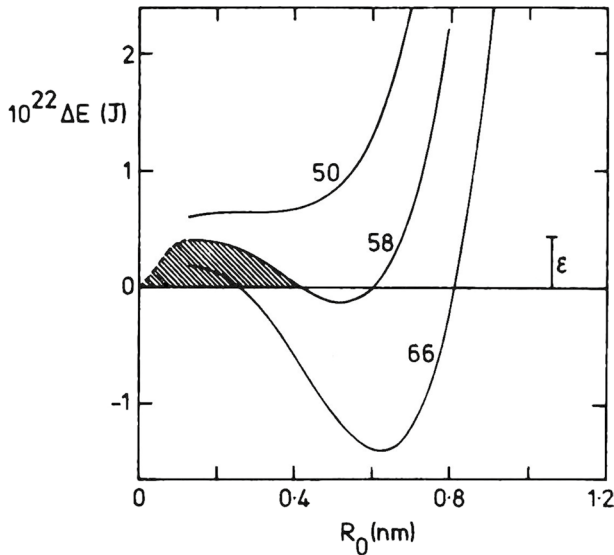


**Fig. 12** Change in energy  $\Delta E$  at constant impulse that occurs when a vortex loop of radius  $R_0$  is formed in the equatorial plane by a negative ion, for the three different ionic velocities (meters per second) shown by the numbers adjacent to the curves (see Sect. 3) [50]. The energy barrier for the case of an ion that slightly exceeds the critical velocity (middle curve) is the hatched area; the part for values of  $R_0$  lower than those for which the calculations of Sect. 3 are valid, and the dashed line, are just sketched as guides to the eye. As noted in Sect. 3.6, the energy barrier must go to zero as the loop radius goes to zero, so this extrapolation is reasonable. The experimental barrier height  $\varepsilon$  deduced from the data of Fig. 11 is indicated by the bar. Reprinted figure with permission, from Hendry et al. [50]. Copyright (1988) by the American Physical Society

$\xi = \hbar / \sqrt{m_4 n g}$ , called the healing length—a characteristic length scale of the condensate representing the distance at which kinetic energy and interaction energy are balanced.

At distances larger than  $\xi$ , the quantum pressure is negligible compared to the ordinary pressure [51], and the condensate behaves like a solution of the classical Euler equation for an inviscid compressible irrotational fluid. At distances smaller than  $\xi$ , the quantum pressure becomes dominant and is responsible for effects which are outside the realm of classical Euler dynamics, such as vortex reconnections and vortex nucleation, as we shall see.

Vortex nucleation by a moving ion and the onset of drag were first demonstrated in the context of the GPE by Frisch et al. [52]. They solved Eq. (28) in two-dimensions (2D) around a disk of diameter  $d = 10\xi$  moving at constant velocity  $v$  (for convenience they performed the calculation in the frame of reference of the disk). They imposed the boundary condition  $\psi = 0$  at the surface of the disk, thus modelling the ion as an infinite potential well. An annular region of thickness  $\approx \xi$  forms around the disk (the superfluid analog of a laminar boundary layer) where the density drops from its bulk value far from the disk to zero at the disk's surface. Frisch et al. found that at small velocities  $v$ , the flow around

the disk is symmetric fore and aft, and frictionless; however, if  $v$  is larger than a critical velocity  $v_c \approx 0.4c$  (where  $c = \sqrt{n_0 g/m_4}$  is the speed of sound in the bulk where the density is  $n_0 = \mu/g$ ), the disk experiences a drag force. The onset of drag for  $v \geq v_c$  is accompanied by the nucleation of vortex-antivortex pairs at the opposite sides of the disk, where the local velocity is the highest. It is therefore convenient to use the Mach number  $M = v/c$  as the control parameter of the problem. The critical Mach number  $M_c = v_c/c$  is less than unity because the nucleation takes place in the annular region of depleted density  $n < n_0$  around the disk where the local speed of sound is reduced compared to the value in the bulk.

Frisch et al. found that in the laboratory frame, each vortex pair moves slower than the disk; the vortex pair is therefore left behind as shown in Fig. 13, and a second pair is nucleated. Increasing  $v$ , this vortex shedding becomes more frequent, time dependent (including the alternating vortices of the von Karman vortex street) and then irregular. This is because each vortex depresses the total velocity near the disk, preventing the nucleation of the next vortex until the mainstream velocity value  $v$  is recovered at which the next nucleation can take place.

Different energy branches of solutions of the GPE were computed by Huepe and Brachet [54] and Mueller and by Krstulovic [55], who determined stable (stationary) and unstable solutions using a Newton-Raphson method. Figure 14 shows a schematic example of their findings in the form of a bifurcation diagram: the quantity  $\Delta E = E(v) - E(0)$ , plotted as a function of the Mach number for a prescribed disk diameter, is used to characterize different solution branches, where  $E(v)$  and  $E(0)$  are, respectively, the energy of the condensate at velocities  $v > 0$  and  $v = 0$ . The solid black line is the stable branch which corresponds to frictionless stationary flow without vortices, and the dashed black line is the unstable branch corresponding to a vortex-antivortex pair. The other energy branches correspond to unstable solutions with two (dashed black line), four (dashed red line) and six (dot-dashed line) nucleated vortices. For a given disk diameter, such a bifurcation diagram allows the identification of the critical Mach number  $M_c$  at the cusp where stable and unstable branches merge. For  $M > M_c$  there are no stationary solutions and the disk nucleates vortices experiencing a drag force. The precise value of  $M_c$  depends on the disk's size  $d$ : as  $d$  increases, the critical Mach number  $M_c$  decreases.

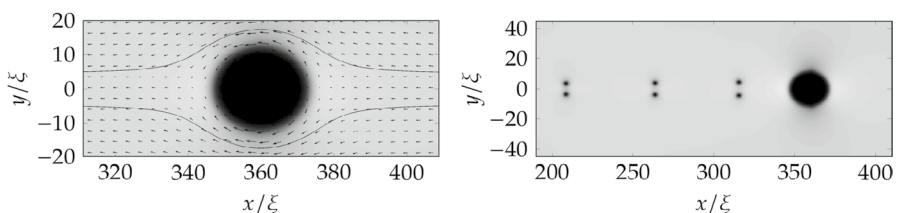


**Fig. 13** Density  $n(x, y)$  vs  $x, y$  corresponding to flow of the condensate around a 2D disk [53]. Dark regions correspond to  $n = 0$ , light regions to the bulk density  $n = n_0$ . The flow is from right to left with speed  $v$ . Left: subcritical flow ( $v = 0.3c < v_c$  where  $c$  is the speed of sound in the bulk; the critical velocity is  $v_c = 0.36c$ ): the flow is frictionless and fore-aft symmetric, like classical potential flow. Right: mildly supercritical flow ( $v = 0.365c > v_c$ ): quantum vortices are shed behind the disk. Reprinted figure, with permission from Stagg [53]

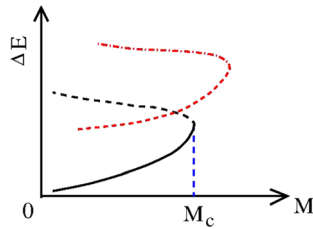


**Fig. 14** Schematic bifurcation diagram of the solutions of the GPE corresponding to flow at speed  $v$  around a disk of diameter  $d$ . The quantity  $\Delta E$  represents solution branches as a function of the Mach number,  $M = v/c$  [54, 55]. The bottom black line is the stable branch corresponding to frictionless motion without vortices; this branch terminates at the critical Mach number  $M_c$ . The other branches are unstable solutions: the dashed black line corresponds to two vortices, the dashed red line to four vortices, and the dot-dashed red line to six vortices. There are no stable solutions for  $M > M_c$  (Color figure online)

Qualitatively, this 2D nucleation scenario is also seen in 3D calculations (the vortex-antivortex pairs being replaced by vortex rings) and in variants of the problem (the ion can be modelled either as a hard object or as a penetrable object; it can be held fixed or have its own dynamics) resulting in slightly different values of  $M_c$  [54, 56, 57].

In particular, the 3D calculation of Winiecki et al. [58] included the backreaction of the flow onto the ion (modelled as a hard object), which makes the ion change velocity at the moment of nucleation. They noticed that the encircling vortex ring which first appears at the equator (corresponding to the vortex-antivortex pair nucleated at the opposite poles in 2D) is unstable, and quickly re-attaches to the sphere, forming a vortex loop which then grows, as shown in Fig. 15; this result is in agreement with the MVD scenario which favors the attached loop as the starting “proto-vortex”. The same effect was noticed by Vilhois and Salman [59] who modelled the ion bubble with a linear Schroedinger equation in the adiabatic approximation, allowing for bubble deformations. In their 3D calculation, they also noticed that, if the driving electric field is large enough, the ion alternates accelerations and decelerations while chaotically shedding and recapturing vortex rings.

## 5.2 The Nonlocal Gross–Pitaevskii Equation

It must be stressed that the Gross–Pitaevskii equation is only a qualitative model of superfluid helium, which is a liquid, not a dilute gas (the condensate is only a fraction of the superfluid density, as we said in Sect. 1). In the GPE, the excitations of the uniform ground state of density  $n_0$  have energy

$$E = \sqrt{\frac{p^4}{4m_4^2} + \frac{n_0 g p^2}{m_4}}, \quad (29)$$

This dispersion relation is consistent with the phonon branch ( $E \propto p$  for  $p \rightarrow 0$ ) of the Landau dispersion curve, but increases quadratically ( $E \propto p^2$ ) at large  $p$ , thus lacking helium’s characteristic roton minimum, as shown by the dashed line



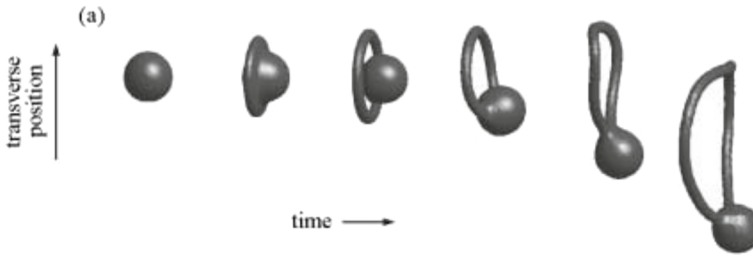


**Fig. 15** Three-D contour plots of the condensate's density at different times [58]. The vortex nucleates as an encircling ring (equivalent to Fig. 13) but the ring is unstable and moves to the side, forming an attached vortex loop. Reprinted figure with permission, from Winiiecki and Adams [58]. Copyright (2000) by *Europhysics Letters*

in Fig. 1. As a consequence, the Landau critical velocity predicted from Eq. (29) is  $v_c = \min(E/p) = \sqrt{n_0 g/m_4} = c$ , corresponding to the process of vortex nucleation described by Frisch et al. [52], which gives too large a value when applied to helium, where  $c \approx 238$  m/s.

To bring the condensate model closer to the physics of superfluid helium, Berloff followed a suggestion of C.A. Jones. She proposed [60, 61] to use Eq. (26) choosing a convenient interaction potential  $U(|\mathbf{x} - \mathbf{x}'|)$  so that the resulting dispersion relation matches the Landau dispersion relation. More precisely, this potential was

$$U(|\mathbf{x} - \mathbf{x}'|) = (\alpha + \beta A^2 r^2 + \delta A^4 r^4) e^{-A^2 r^2}. \quad (30)$$

where  $r = |\mathbf{x} - \mathbf{x}'|$ . An extra nonlinear term proportional to  $\psi|\psi|^{2(1+\gamma)}$ , representing beyond-mean field corrections, was also added to Eq. (26) to prevent focusing instabilities. The resulting equation (which for simplicity here we do not write fully) is now called the “nonlocal” Gross–Pitaevskii equation. The coefficients  $\alpha$ ,  $\beta$ ,  $\gamma$ ,  $\delta$  and  $A$  are chosen so that its dispersion relation is a good fit to the Landau dispersion curve of superfluid helium (meaning the observed sound speed at small  $p$  and the correct roton minimum at large  $p$ ) [62].

Recently, Mueller and Krstulovic [55] used the nonlocal GPE to determine the critical velocity of vortex nucleation by a moving 2D disk. Given a small disk size, e.g.,  $d = 10\xi$ , they found that the stable branch (which, for the ordinary GPE, would be the solid black line of Fig. 14) terminates abruptly at the critical Mach number  $M_c = 0.25$  which hereafter we call  $M_L$ , in agreement with the Landau critical velocity  $v_L \approx 60$  m/s. When the disk's Mach number is larger than  $M_L$ , they observed the emission of density oscillations with the wavenumber of rotons, without any vortex nucleation; vortex nucleation appears at a larger Mach number and, as for the ordinary GPE, it depends on  $d$ . Their results are summarized schematically in Fig. 16. If  $d < 100\xi$ , there is a range of Mach numbers ( $M_L < M < M_c$ ) where the disk emits rotons but does not nucleate vortices. For  $d > 100\xi$ , vortex nucleation is accompanied by roton emission. The dependence of  $M_c$  on the obstacle's size is significant for relatively large obstacles. For

$d \gg \xi$ , the critical Mach number  $M_c$  is less than  $M_L$  and decreases with increasing  $d$ . The fact that the curves of the critical Mach number  $M_c$  versus  $d/\xi$  for the ordinary GPE and the nonlocal GPE become essentially the same at large  $d/\xi$  suggests that rotons are irrelevant to vortex nucleation by large objects. Practical computing limitations prevented calculations for the typical size of obstacles used in experiments. For example, Efimov et al. [63] used vibrating forks of size  $d \approx 0.4 \text{ mm} \approx 4 \times 10^6 \xi$ , which is four orders of magnitude larger than the largest disk side which Mueller and Krstulovic could compute. In this experiment, Efimov et al. observed a critical velocity  $v_c \approx 10 \text{ cm/s}$ , which corresponds to  $M_c \approx 4.2 \times 10^{-4}$  (clearly far too much to the bottom and to the right in Fig. 16 to calculate).

In conclusion, the nonlocal variant of the GPE has brought the condensate model into better agreement with the physics of liquid helium than the original (local) GPE, in the sense that the model now contains roton excitations and predicts the correct value for the Landau critical velocity. However, the effect of changing the pressure on the roton/vortex nucleation has not yet been investigated.

## 6 Conclusions

The good agreement between the MVD calculations [24] reviewed in Sect. 3 and the experiments [12] described in Sect. 4 vindicated Vinen's intuition [35] that an energy barrier impedes the nucleation of vortices in superfluid  $^4\text{He}$  and that, quite generally, the vortex nucleation problem is important. This conclusion is

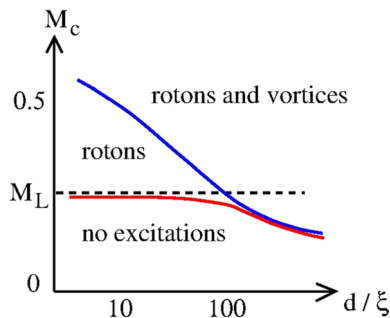


**Fig. 16** Schematic critical Mach number  $M_c$  as a function of the disk's diameter,  $d$ , computed by Mueller and Krstulovic [55] using the nonlocal GPE. Note that the horizontal axis is logarithmic. The horizontal dashed line marks the Mach number  $M_L \approx 0.25$  corresponding to the Landau critical velocity  $v_L \approx 60 \text{ m/s}$  computed for the dispersion curve with rotons. The red curve and the blue curve mark, respectively, the thresholds for creation of roton excitations and vortices. For  $d < 100\xi$  there is a region of Mach numbers (between the red line and the blue line) in which the moving obstacle creates rotons but no vortices. For  $d > 100\xi$ , roton radiation and vortex nucleation happen together. In contrast, in the ordinary GPE model, the blue curve remains essentially the same, the red curve is absent, and  $M_L$ , predicted by Landau's argument for a dispersion curve without rotons, is higher ( $M_L = 1$ ) (Color figure online)

strengthened by follow-up studies, described in Sect. 5, in which, lacking a better microscopic model of superfluid helium, Gross–Pitaevskii theory has been applied to illuminate the dynamics of the nucleation mechanism.

There has also been significant experimental progress since Vinen’s original work. For example, a filtering technique [64] has been developed which achieves a  $^4\text{He}$  sample effectively free of remanent vortex lines. Above all, the existence of critical velocities has been studied in other quantum fluids, notably  $^3\text{He}$  [65], atomic Bose–Einstein condensates [66] and polariton condensates [67]. The Karman vortex street, predicted for ion velocities exceeding the nucleation velocity of the first vortex pair, has been observed in atomic condensates [68, 69] and further analyzed [70], leading to a better understanding of vortex clustering and the classical inverse energy cascade [71]; the effects of density inhomogeneities [57, 72, 73], particularly important for atomic condensates, have been considered.

Finally, it is worth remarking that a dynamical model like the GPE, which, although simplified, includes vortex nucleation, has opened the way to study small-scale superfluid motions near a boundary which are still inaccessible to low temperature flow visualization. One example is the detailed formation of a vortex lattice inside a rotating cylinder [74]: small vortex loops nucleate on the boundary’s roughness (for all experimental boundaries are “rough” on the scale of the healing length of  $^4\text{He}$ ), grow, interact, and, after a brief transient turbulent state, settle down into a regular vortex array. Another example is the prediction of a turbulent boundary layer created by a superflow flowing past a rough boundary [75]. The legacy of Vinen’s intuition runs deep.

**Acknowledgements** We freely acknowledge our enormous indebtedness to Joe Vinen, with whom we all collaborated in different ways over many years. It was a privilege to do so, and it enhanced our development as scientists. We greatly miss the cut-and-thrust of scientific discussion with him, his penetrating insights into the natural world, and his fascination and enthusiasm for physics.

**Author Contributions** All authors contributed equally to the preparation of the manuscript.

**Funding** This research was supported by: the Engineering and Physical Sciences Research Council (United Kingdom) under grants Nos. EP/P022197/1 “Microscopic dynamics of quantized vortices in turbulent superfluid in the  $T = 0$  limit” and EP/X004597/1 “Creation and evolution of quantum turbulence in novel geometries”; and by the UKRI (UK Research and Innovation) under grant “Quantum simulators for fundamental physics” (ST/t006900/1)

## Declarations

**Competing interests** The authors have no financial or non-financial conflicts of interests to disclose that are directly or indirectly related to the work.

**Open Access** This article is licensed under a Creative Commons Attribution 4.0 International License, which permits use, sharing, adaptation, distribution and reproduction in any medium or format, as long as you give appropriate credit to the original author(s) and the source, provide a link to the Creative Commons licence, and indicate if changes were made. The images or other third party material in this article are included in the article’s Creative Commons licence, unless indicated otherwise in a credit line to the material. If material is not included in the article’s Creative Commons licence and your intended use is not permitted by statutory regulation or exceeds the permitted use, you will need to obtain permission directly from the copyright holder. To view a copy of this licence, visit <http://creativecommons.org/licenses/by/4.0/>.

## References

1. P.L. Kapitza, Viscosity of liquid helium below the lambda-point. *Nature* **141**, 74 (1938)
2. J.F. Allen, A.D. Misener, Flow of liquid Helium II. *Nature* **141**, 75 (1938)
3. J. Wilks, *The Properties of Liquid and Solid Helium* (Clarendon Press, Oxford, 1967)
4. J. Wilks, D.S. Betts, *An Introduction to Liquid Helium* (Clarendon Press, Oxford, 1987)
5. R.J. Donnelly, J.A. Donnelly, R.N. Hills, Specific heat and dispersion curve for Helium II. *J. Low Temp. Phys.* **44**, 471–489 (1981)
6. L. Tisza, Transport phenomena in Helium II. *Nature* **141**, 913 (1938)
7. F. London, The  $\lambda$ -phenomena of liquid helium and the Bose–Einstein degeneracy. *Nature* **141**, 643–644 (1938)
8. E. Andronikashvili, in *Helium 4* (translation of *J. Phys. (U.S.S.R.)* **10**, 201; 1946), ed. by Z.M. Galasiewicz (Pergamon, Oxford, 1971), pp. 154–165
9. L.D. Landau, The theory of superfluidity of Helium II. *J. Phys. (USSR)* **5**, 71–90 (1941)
10. L.D. Landau, On the theory of superfluidity of Helium II. *J. Phys. (USSR)* **11**, 91–92 (1947)
11. G.W. Rayfield, Roton emission from negative ions in Helium II. *Phys. Rev. Lett.* **16**(21), 934–936 (1966)
12. D.R. Allum, P.V.E. McClintock, A. Phillips, R.M. Bowley, The breakdown of superfluidity in liquid  $^4\text{He}$ : an experimental test of Landau’s theory. *Philos. Trans. R. Soc. Lond. A* **284**, 179–224 (1977)
13. T. Ellis, P.V.E. McClintock, The breakdown of superfluidity in liquid  $^4\text{He}$ : V. Measurement of the Landau critical velocity for roton creation. *Philos. Trans. R. Soc. Lond. A* **315**, 259–300 (1985)
14. L. Onsager, Statistical hydrodynamics. *Suppl. Nuovo Cimento.* **6**, 279–287 (1949)
15. R.P. Feynman, in *Progress, Low Temperature Physics*, vol. 1, ed. by C.J. Gorter (Elsevier, Amsterdam, 1955), pp. 17–53
16. V.F. Sears, E.C. Svensson, P. Martel, A.D.B. Woods, Neutron-scattering determination of the momentum distribution and the condensate fraction in liquid  $^4\text{He}$ . *Phys. Rev. Lett.* **49**, 279–282 (1982)
17. D.R. Tilley, J. Tilley, *Superfluidity and Superconductivity*, 2nd edn. (Adam Hilger, Bristol, 1986)
18. E.A. Cornell, C.E. Wieman, Nobel lecture: Bose–Einstein condensation in a dilute gas, the first 70 years and some recent experiments. *Rev. Mod. Phys.* **74**, 875–893 (2002)
19. L. Chomaz, R.M.W. van Bijnen, D. Petter, G. Faraoni, S. Baier, J.H. Becher, M.J. Mark, L. Santos, L. Ferlaino, Observation of roton mode population in a dipolar quantum gas. *Nat. Phys.* **14**, 442–446 (2018)
20. H. Deng, H. Haug, Y. Yamamoto, Exciton–polariton Bose–Einstein condensation. *Rev. Mod. Phys.* **82**, 1489–1537 (2010)
21. W.F. Vinen, Detection of single quanta of circulation in liquid Helium II. *Proc. R. Soc. Lond. A* **260**, 218 (1961)
22. V.M.H. Ruutu, U. Parts, J.H. Koivuniemi, N.B. Kopnin, M. Krusius, Intrinsic and extrinsic mechanisms of vortex formation in superfluid. *J. Low Temp. Phys.* **106**, 93–164 (1997)
23. G.W. Rayfield, F. Reif, Quantized vortex rings in superfluid helium. *Phys. Rev. A* **136**, 1194–1208 (1964)
24. C.M. Muirhead, W.F. Vinen, R.J. Donnelly, The nucleation of vorticity in superfluid  $^4\text{He}$ . I. Basic theory. *Philos. Trans. R. Soc. Lond. A* **311**, 433–467 (1984)
25. P.C. Hendry, N.S. Lawson, P.V.E. McClintock, C.D.H. Williams, R.M. Bowley, The breakdown of superfluidity in liquid Helium-4. VI. Macroscopic quantum tunnelling by vortices in isotopically pure He II. *Philos. Trans. R. Soc. Lond. A* **332**, 387–414 (1990)
26. A.P. Finne, V.B. Eltsov, R. Hänninen, N.B. Kopnin, J. Kopu, M. Krusius, M. Tsubota, G.E. Volovik, Dynamics of vortices and interfaces in superfluid  $^3\text{He}$ . *Rep. Prog. Phys.* **69**, 3157–3230 (2006)
27. D.D. Awschalom, K.W. Schwarz, Observation of a remanent vortex-line density in superfluid helium. *Phys. Rev. Lett.* **52**, 49–52 (1984)
28. W.F. Vinen, L. Skrbek, Quantum turbulence generated by oscillating structures. *Proc. Natl. Acad. Sci. (USA)* **111**(Suppl. 1), 4699–4706 (2014)
29. A.L. Fetter, in *The Physics of Liquid and Solid Helium*, part 1, ed. by K.H. Bennemann, J.B. Ketterson (Wiley, New York, 1976), chap. 3
30. Y. Xing, H.J. Maris, Electrons and exotic ions in superfluid Helium-4. *J. Low Temp. Phys.* **201**, 634–657 (2020)

31. D.R. Allum, R.M. Bowley, P.V.E. McClintock, Evidence for roton pair creation in superfluid  $^4\text{He}$ . *Phys. Rev. Lett.* **36**(22), 1313–1316 (1976)
32. J. Poitrenaud, F.I.B. Williams, Precise measurement of effective mass of positive and negative charge-carriers in liquid Helium II. *Phys. Rev. Lett.* **29**(18), 1230–1232 (1972)
33. J. Poitrenaud, F.I.B. Williams, Erratum: Precise measurement of effective mass of positive and negative charge-carriers in liquid Helium II. *Phys. Rev. Lett.* **32**(21), 1213 (1974)
34. T. Ellis, P.V.E. McClintock, R.M. Bowley, Pressure-dependence of the negative-ion effective mass in He II. *J. Phys. C: Solid State Phys.* **16**(15), L485–L489 (1983)
35. W.F. Vinen, *Liquid Helium: Enrico Fermi International School of Physics Course XXI* (Academic Press, New York, 1963), pp.336–355
36. H. Lamb, *Hydrodynamics*, 6th edn. (CUP, Cambridge, 1952)
37. K.W. Schwarz, P.S. Jang, Creation of quantized vortex rings by charge-carriers in superfluid-helium. *Phys. Rev. A* **8**(6), 3199–3210 (1973)
38. C.F. Barenghi, R.J. Donnelly, Vortex rings in classical and quantum systems. *Fluid Dyn. Res.* **41**, 051401 (2009)
39. G.E. Volovik, Quantum-mechanical formation of vortices in a superfluid liquid. *Sov. Phys. JETP Lett.* **15**, 81–83 (1972)
40. E.B. Sonin, Critical velocities at very low temperatures, and the vortices in a quantum Bose fluid. *Sov. Phys. JETP* **37**(3), 494–500 (1973)
41. M. Ichiyanagi, Tunneling critical velocity of a superfluid. *J. Low Temp. Phys.* **23**(5–6), 599–603 (1976)
42. R.M. Bowley, P.V.E. McClintock, F.E. Moss, G.G. Nancolas, P.C.E. Stamp, The breakdown in superfluidity in liquid  $^4\text{He}$ : III. Nucleation of quantised vortex rings. *Philos. Trans. R. Soc. Lond. A* **307**, 201–260 (1982)
43. A.O. Caldeira, A.J. Leggett, Influence of dissipation on quantum tunneling in macroscopic systems. *Phys. Rev. Lett.* **46**(4), 211–214 (1981)
44. R. J. Donnelly, P. H. Roberts, Stochastic theory of the nucleation of quantized vortices in superfluid helium. *Philos. Trans. R. Soc. Lond. A* **271**, 41–100 (1971)
45. S. Liu, G. Labbe, G.G. Ihas, Producing towed grid quantum turbulence in liquid  $^4\text{He}$ . *J. Low Temp. Phys.* **148**, 281–285 (2007)
46. D.I. Bradley, M. Človečko, M.J. Fear, S.N. Fisher, A.M. Guénault, R.P. Haley, C.R. Lawson, G.R. Pickett, R. Schanen, V. Tsepelin, P. Williams, A new device for studying low or zero frequency mechanical motion at very low temperatures. *J. Low Temp. Phys.* **165**, 114 (2011)
47. D.E. Zmeev, A method for driving an oscillator at a quasi-uniform velocity. *J. Low Temp. Phys.* **175**, 480–485 (2014)
48. M. Arrayás, J.L. Trueba, C. Uriarte, D.E. Zmeev, Design of a system for controlling a levitating sphere in superfluid  $^3\text{He}$  at extremely low temperatures. *Sci. Rep.* **11**, 20069 (2021)
49. G.G. Nancolas, R.M. Bowley, P.V.E. McClintock, The breakdown of superfluidity in liquid He-4: IV. Influence of He-3 isotopic impurities on the nucleation of quantized vortex rings. *Philos. Trans. R. Soc. Lond. A* **313**, 537–610 (1985)
50. P.C. Hendry, N.S. Lawson, P.V.E. McClintock, C.D.H. Williams, R.M. Bowley, Macroscopic quantum tunnelling of vortices in He II. *Phys. Rev. Lett.* **60**, 604–607 (1988)
51. C.F. Barenghi, N.G. Parker (eds.), *A Primer on Quantum Fluids* (Springer, Berlin, 2016)
52. T. Frisch, Y. Pomeau, S. Rica, Transition to dissipation in a model of superflow. *Phys. Rev. Lett.* **69**, 1644–1647 (1992)
53. G.W. Stagg, *A Numerical Study of Vortices and Turbulence in Quantum Fluids*. Ph.D. thesis, Newcastle University (2016)
54. C. Huepe, M.E. Brachet, Scaling laws for vortical nucleation solutions in a model of superflow. *Phys. D* **140**, 126–140 (2000)
55. N.P. Müller, G. Krstulovic, Critical velocity for vortex nucleation and roton emission in a generalized model for superfluids. *Phys. Rev. B* **105**, 014515 (2022)
56. N.G. Berloff, P.H. Roberts, Motions in a Bose condensate: VII. Boundary-layer separation. *J. Phys. A: Math. Gen.* **33**, 4025–4038 (2000)
57. T. Winiecki, B. Jackson, J.F. McCann, C.S. Adams, Vortex shedding and drag in dilute Bose–Einstein condensates. *J. Phys. B: At. Mol. Opt.* **33**, 4069–4078 (2000)
58. T. Winiecki, C.S. Adams, Motion of an object through a quantum fluid. *Europhys. Lett.* **52**, 257–263 (2000)

59. A. Villois, H. Salman, Vortex nucleation limited mobility of free electron bubbles in the Gross–Pitaevskii model of a superfluid. *Phys. Rev. B* **97**, 094507 (2018)
60. N.G. Berloff, Nonlocal nonlinear Schroedinger equations as models of superfluidity. *J. Low Temp. Phys.* **116**, 359 (1999)
61. N.G. Berloff, P.H. Roberts, Motions in a Bose condensate: VI. Vortices in a nonlocal model. *J. Phys. A: Math. Gen.* **32**, 5611–5625 (1999)
62. S. Villerot, B. Castaing, L. Chevillard, Static spectroscopy of a dense superfluid. *J. Low Temp. Phys.* **169**, 1–14 (2012)
63. V.B. Efimov, D. Garg, O. Kolosov, P.V.E. McClintock, Direct measurement of the critical velocity above which a tuning fork generates turbulence in superfluid helium. *J. Low Temp. Phys.* **158**(3/4), 456–461 (2010)
64. N. Hashimoto, R. Goto, H. Yano, K. Obara, O. Ishikawa, T. Hata, Control of turbulence in boundary layers of superfluid He-4 by filtering out remanent vortices. *Phys. Rev. B* **76**(2), 020504 (2007)
65. J.M. Parpia, J.D. Reppy, Critical velocities in superfluid  $^3\text{He}$ . *Phys. Rev. Lett.* **43**, 1332–1336 (1979)
66. C. Raman, M. Kohl, R. Onofrio, D.S. Durfee, C.E. Kuklewicz, Z. Hadzibabic, W. Ketterle, Evidence for a critical velocity in a Bose–Einstein condensed gas. *Phys. Rev. Lett.* **83**, 2520 (1999)
67. I. Carusotto, C. Ciuti, Quantum fluids of light. *Rev. Mod. Phys.* **85**, 299 (2013)
68. K. Sasaki, N. Suzuki, H. Saito, Bénard von Karman vortex street in a Bose–Einstein condensate. *Phys. Rev. Lett.* **104**, 150404 (2010)
69. W.J. Kwon, J.H. Kim, S.W. Seo, Y. Shin, Observation of von Karman vortex street in an atomic superfluid gas. *Phys. Rev. Lett.* **117**, 245301 (2016)
70. G.W. Stagg, N.G. Parker, C.F. Barenghi, Quantum analogues of classical wakes in Bose–Einstein condensates. *J. Phys. B: At. Mol. Opt. Phys.* **47**, 095304 (2014)
71. M.T. Reeves, T.P. Billam, B.P. Anderson, A.S. Bradley, Inverse energy cascade in forced two-dimensional quantum turbulence. *Phys. Rev. Lett.* **110**, 104501 (2013)
72. B. Jackson, J.F. McCann, C.S. Adams, Vortex formation in dilute inhomogeneous Bose–Einstein condensates. *Phys. Rev. Lett.* **80**, 3903 (1998)
73. K. Fujimoto, M. Tsubota, Nonlinear dynamics in a trapped Bose–Einstein condensate induced by an oscillating Gaussian potential. *Phys. Rev. A* **83**, 053609 (2011)
74. N.A. Keepfer, G.W. Stagg, L. Galantucci, C.F. Barenghi, N.G. Parker, Spin-up of a superfluid vortex lattice driven by rough boundaries. *Phys. Rev. B* **102**, 144520 (2020)
75. G.W. Stagg, N.G. Parker, C.F. Barenghi, Superfluid boundary layer. *Phys. Rev. Lett.* **118**, 135301 (2017)

**Publisher's Note** Springer Nature remains neutral with regard to jurisdictional claims in published maps and institutional affiliations.